John von Neumann Institute for Computing

Mash-Free Simulation of High Intensity Laser Interactions with Collisional Plasmas

Paul Gibbon

published in

NIC Symposium 2006 ,
G. Münster, D. Wolf, M. Kremer (Editors),
John von Neumann Institute for Computing, Jülich,
NIC Series, Vol. **32**, ISBN 3-00-017351-X, pp. 333-340, 2006.

http://www.fz-juelich.de/nic-series/volume32

Mesh-Free Simulation of High Intensity Laser Interactions with Collisional Plasmas

Paul Gibbon

Central Institute for Applied Mathematics
Research Centre Jülich, 52425 Jülich, Germany
E-mail: p.gibbon@fz-juelich.de

The acceleration and transport of energetic particles produced by high intensity laser interaction with solid targets is studied using a recently developed plasma simulation technique. Based on a parallel tree algorithm, this method provides a powerful, mesh-free approach to numerical plasma modelling, permitting 'whole target' investigations without the need for artificial particle and field boundaries. Moreover, it also offers a natural means of treating three-dimensional, collisional transport effects hitherto neglected or suppressed in conventional explicit particle-in-cell simulation. Multi-million particle simulations of this challenging interaction regime using the code PEPC (Pretty Efficient Parallel Coulomb-solver: `http://www.fz-juelich.de/zam/pepc`) have been performed on the JUMP and BlueGene/L computers for various open-boundary geometries. These simulations highlight the importance of target resisitivity and surface effects on the fast electron current flow.

1 Introduction

Numerical simulation of hot, ionized matter poses a constant challenge to the plasma theorist because of the effectively unlimited degrees of freedom, extreme nonlinear behaviour and vast range of length- and timescales characteristic of both natural and laboratory plasmas. Usually, the intractability of first-principles simulation is overcome by first simplifying the problem in phase space; replacing individual particle trajectories by a smooth velocity distribution and then solving a Vlasov-Boltzmann-type equation. By formal application of kinetic theory, many problems can be further reduced to the magnetohydrodynamics picture – the plasma equivalent of the Navier-Stokes equations. Whether particle or fluid, virtually all plasma modelling over the past four decades has relied on a spatial mesh to mediate the interplay between plasma particles and their self-consistent electric and magnetic fields. While these models have proved highly successful, the presence of a grid ultimately places restrictions on the spatial resolution or geometry which can be considered – especially in three dimensions.

In the Computer Simulations Division at ZAM, a new mesh-free plasma simulation paradigm has been developed which overcomes some of these limitations. Inspired by the N-body tree algorithms designed to speed up gravitational problems in astrophysics[1], this approach reverts to first principles by computing forces on individual particles directly, following their trajectories in a Lagrangian, 'molecular dynamics' fashion[2]. We have now combined this technique with a finite-sized-particle (FSP) model to study particle transport in high-intensity laser-plasma interactions, a field of fundamental importance to future compact laser-based particle and radiation sources[3].

2 Lagrangian Finite-Sized-Particle Kinetics

We first give a brief description of the electrostatic FSP model as currently implemented in PEPC: a generalisation of this scheme to include self-generated magnetic fields and a set of radiation-free Maxwell equations will be presented elsewhere. The choice of units is somewhat subtle for macroscopic mesh-free plasma simulation, and contrasts with the microscopic 'Debye' system used, for example in previous work[2]. The quantities time, space, velocity, charge and mass are normalized to $\omega_p^{-1}, c\omega_p^{-1}, c, N_p e, N_p m_e$ respectively, so that the equation of motion for a particle i with charge q_i and mass m_i becomes:

$$m_i \frac{d\boldsymbol{u}_i}{dt} = \frac{1}{3} q_i \sum_{i \neq j} \frac{q_j \boldsymbol{r}_{ij}}{(r_{ij}^2 + \varepsilon^2)^{3/2}} + q_i \boldsymbol{E}^p(\boldsymbol{r}_i), \tag{1}$$

where $\boldsymbol{r}_{ij} = \boldsymbol{r}_i - \boldsymbol{r}_j$ is the separation between particles i and j, and $\boldsymbol{u}_i = \gamma \boldsymbol{v}_i$ is its proper velocity; $\gamma = (1 + \mid \boldsymbol{u} \mid^2 / c^2)^{1/2}$ the relativistic factor. We have also added an external field $\boldsymbol{E}^p$, and made use of the plasma frequency definition, $\omega_p^2 = 4\pi e^2 n_e / m_e$ for electron density n_e. The constant N_p is thus eliminated by setting:

$$N_p = \frac{4\pi}{3} n_e \left(\frac{c}{\omega_p} \right)^3 .$$

In a tree code, the $O(N)$ sum over all other particles is replaced by a sum over *multipole* expansions (expanded here up to quadrupole) of groups of particles, whose size increases with distance from particle i. The number of terms in this sum is $O(\log N)$, which even after the additional overhead in computing the multipoles, results in a substantial saving in effort for large N[4].

As in classical MD simulation, we cannot use the pure Coulomb law for point charges because of the finite timestep, which will cause some particles to experience large, stochastic jumps in their acceleration, eventually destroying the energy conservation. We therefore include a softening parameter ε in Eq. (1) to ensure that $\boldsymbol{E}(\boldsymbol{r}) \to 0$ as $r \to 0$. Physically, we no longer have point charges, but rather charge clouds with a smooth charge density. It is instructive to compute the latter by applying Gauss' law to (1) with $\boldsymbol{E}^p = 0$, giving (density normalized to en_e):

$$\rho(r) = \frac{q\varepsilon^2}{(r^2 + \varepsilon^2)^{5/2}} \tag{2}$$

Charge assignment is then straightforward: the total charge contained within a cuboid volume $V = x_L \times y_L \times z_L$ (in normalized units) is

$$Q = \sum_i q_i = \rho_0 V = N_e Q_s,$$

where N_e is the total number of simulation electrons and Q_s is the macro-charge carried by them. Since the initial density $\rho_0 = -1$, we simply have $Q_s = -\frac{V}{N_e}$. Assigning charges Q_s and $-Q_s Z$ to the electrons and ions respectively, and masses $M_s^e = |Q_s|, M_s^i = A|Q_s|$, where Z and A are the atomic number and mass, sets up a macroscopic plasma system whose internal dynamics is governed solely by Equation 1.

One can show that the effective collision frequency for this system of finite-sized cloud charges is given by:[5,6]

$$\frac{\nu_c}{\omega_p} \simeq \frac{Z}{30N_D}\left(\frac{\lambda_D}{\varepsilon}\right)^2 = \frac{Z}{30N_c}\left(\frac{\varepsilon}{\lambda_D}\right), \tag{3}$$

where $N_c = \frac{4\pi}{3} n_e \varepsilon^3$ (the number of particles within the cloud radius) and λ_D is the Debye length.

Since electromagnetic wave propagation cannot be included in the present (electrostatic) model, a ponderomotive standing wave ansatz for the laser field E_L is applied at the vacuum-plasma boundary on the front-side of the target. Essentially the laser field is represented by a relativistic potential

$$\gamma_p = (1 + \Psi)^{1/2},$$

where

$$\Psi = 4a_0^2 X^2(x) R(r) T(t), \tag{4}$$

where a_0 is the normalized laser pump strength and $X(x), R(r)$ and $T(t)$ are the longitudinal, radial and temporal components determined by (analytically) solving the Helmholtz equations for a density step-profile[7].

The radius $r = (y^2 + z^2)^{1/2}$ is taken relative to the center of the focal spot. This form is used in order to create a sharp radial cutoff at $r = 2\sigma_L$ (σ_L is the *half*-width, half-maximum of the laser spot). The time-dependent component $T(t)$ provides both the $j \times B$ heating and DC push on the electron density. Finally, the longitudinal and radial ponderomotive field components (applied as external forces in the momentum equation for the electrons) are found from $E_x^p = d\gamma_p/dx$ and $E_r^p = d\gamma_p/dr$ respectively. Despite its obvious simplicity, this model exhibits surprisingly good agreement with one-dimensional, electromagnetic PIC simulations in terms of the field structure, fast electron heating and ion shock dynamics, provided the electron density scale-length L remains small compared to the laser wavelength λ .

3 Proton Acceleration in Resistive Targets

In contrast to standard particle-in-cell simulations[8], the finite electrical conductivity of the target can be included quite easily within FSP model. Previous theoretical[9] and experimental[10] work has demonstrated that resistive effects already inhibit hot electron penetration for intensities as low as 10^{17} Wcm^{-2} . The Spitzer resistivity can be related to the effective collision frequency $\tilde{\nu}_{ei} \equiv \nu_c/\omega_p$ used in the model (Eq. 3) simply via:

$$\begin{aligned} \eta_e &= \frac{m_e \nu_{ei}}{n_e e^2} = \frac{1}{\omega_p \varepsilon_0}\tilde{\nu}_{ei} \qquad \text{(SI)} \\ &= 6.3 \times 10^{-6} n_{23}^{-1/2} \tilde{\nu}_{ei} \quad \Omega\,\text{m}, \end{aligned} \tag{5}$$

where n_{23} is the electron density in units of 10^{23} cm^{-3}.

To illustrate how the inhibition of electron transport affects ion acceleration, we compare two simulations with different target conductivities but otherwise identical parameters: $I\lambda^2 = 2.5 \times 10^{19}$ Wcm$^{-2}\mu$m^2 ($a_0 = 4$), $\sigma_L = 15\ c/\omega_p$, (square) pulse duration

$\tau_L = 100$ fs and initial plasma density $n_0/n_c = 4$. The initial electron temperatures in the two cases are 5 keV and 500 eV; the particle diameters $\varepsilon = 3$ and 0.7, giving effective normalized resistivities $\tilde{\eta}_e \equiv \tilde{\nu}_{ei} = 7 \times 10^{-3}$ and 0.45 respectively.

In the high-temperature case, the effective hot electron range determined by electrostatic stopping is[9] $R_h \approx 80$ μm, so we expect the simulation to behave much like a collisionless PIC code would. This is just what we observe in Fig. 1, which shows three-dimensional snapshots of the ion density and hot electron temperature. This first plot encapsulates many of the salient features of high-intensity interactions familiar from 2- and 3D PIC simulations to date: bursts of $j \times B$-accelerated electrons generated at 2ω freely traversing the target; formation of a ponderomotively driven ion shock on the front side; and a hot electron Debye sheath being formed on the rear side, pulling ions away from the surface. We also find that the whole foil has been heated to over 50 keV in under 100 fs, in agreement with PIC simulations.

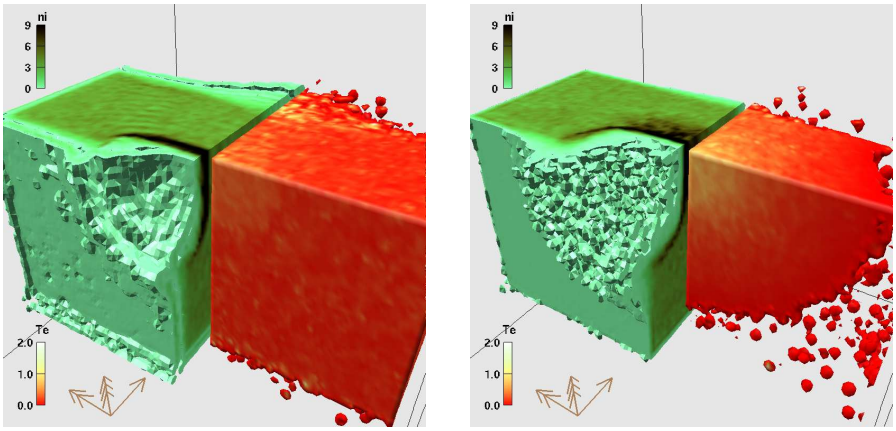

Figure 1. Isovolume sequences of ion density (left; threshold $n_c/20$) and mean electron energy (right; threshold $U_h \geq 10$ keV) sliced half-way through the target in the xz-plane for targets with initial normalized resistivities of a) $\overline{\eta}_e = 7 \times 10^{-3}$ and b) $\overline{\eta}_e = 0.45$ at a time $\omega_p t = 650$ (170 fs).

Comparing this now with Fig. 1b), a similar sequence for the 500 eV 'resistive' simulation for which the effective hot electron range is now reduced to $R_h \approx 1.2$ μm by electrostatic inhibition. This time we see a completely different picture: despite having energies in the MeV range, the hot electrons are confined to a hemispherical heat-front, 1–2 μm ahead of the shock and are virtually absent from the rear-side vacuum region at this time. This is consistent with analytical models[9] and 2D Fokker-Planck simulations[11], which predict a *diffusive* rather than free-streaming behaviour at intensities high enough to induce electrostatic transport inhibition.

The consequences of hot electron transport inhibition for the proton acceleration are dramatic: the absence (or significantly delayed presence) of the hot Debye sheath on the rear side clearly suppresses ion acceleration there[6]. On the other hand, the resistively induced electric field in front of the shock will act to enhance the front-side acceleration. These observations are summarized in Fig. 2, which shows how the relative maximum

energy of protons originating from the front and rear of the foil respectively *reverses* as the target resistivity is increased.

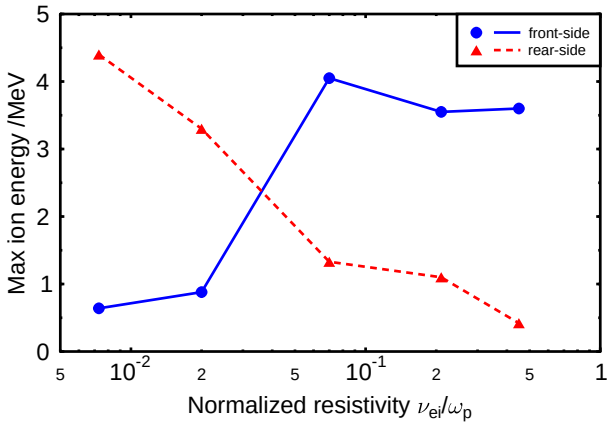

Figure 2. Maximum energy in MeV of protons originating from the front (solid line) and rear (dashed line) of the foil at 150 fs as a function of target resistivity.

4 Mass-Limited Targets

One of the problems in modelling laser-solid interactions at ever higher intensities is that the particle fluxes become so large that the periodic or reflective boundary conditions which are usually applied start to acquire dubious validity. By contrast, the present model sidesteps this issue completely: particles are permitted to fly freely away from and around the target surface. This feature is essential when modelling 'mass-limited' or mesoscopic targets, such as atomic clusters or thin wires.

An example of a laser interaction with a 1 μm -radius wire target is depicted in Fig. 3, which shows a sequence of ion density iso-volumes, but this time consisting of a 1/2-wire vertical slice. Superimposed on these plots are slices of the instantaneous electron temperature, showing that while the laser is incident, the hottest electrons are actually confined to the shock region (a,b). At the same time, there is also a strong circulation of hot electrons *around* the wire.

A striking feature of this simulation is that the entire mid-section of the wire is pushed out by the laser: the beamlet visible in Fig. 3d) has detached itself completely from the wire and continues to propagate away, spreading as it does so. This is reminiscent of three-dimensional PIC simulations of double-layer targets in which a proton beam was created from the low-Z coating on the *rear*-side[12]. By contrast, the main push in this case comes unmistakably from the target front side, even though the beamlet comprises ions which originate from across the whole wire. A further outcome of simulations in this geometry is a disc-like component in the ion emission appearing at later times – also observed in recent experiments[13,14].

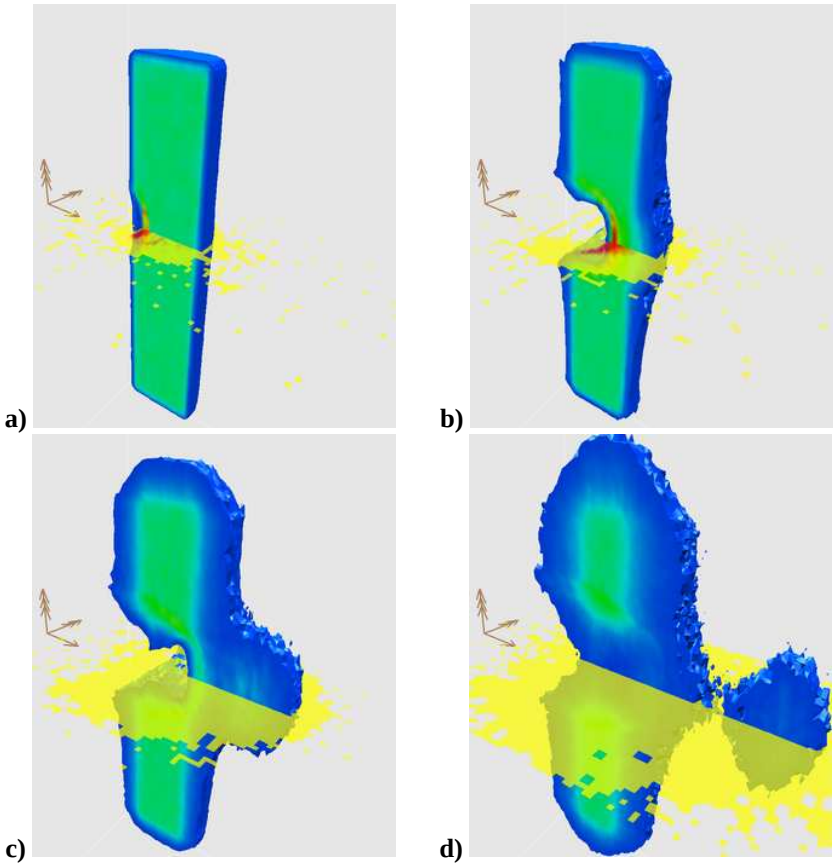

Figure 3. Time-sequence of ion density iso-volume $n_i/n_c \geq 0.25$ and electron temperature T_e slice in plane of laser incidence for a 1/2 wire-section sliced along the wire z-axis. Times shown are a) 200/ω_p , b) 400/ω_p , c) 600/ω_p and d) 800/ω_p .

5 Performance

The examples shown here were set up with between 2 and 6 million electrons and ions uniformly distributed in targets with dimensions $12 \times 12 \times 5$ μm^3. A typical simulation for a 100fs laser pulse would consume 5000 hours on a single Power4 CPU, but this reduces to around 50 wall-clock hours when run on 192 processors of the JUMP machine. By far the most algorithmically demanding part of this code is the tree walk, which in PEPC combines a previous list-based vectorised algorithm[15] with the asynchronous scheme of Warren & Salmon[16] for requesting multipole information on-the-fly from non-local processor domains. In the present scheme, rather than performing complete traversals for one particle at a time, as many 'simultaneous' traversals are made as possible, thus maximising the communication bandwidth by bundling multipole-swaps via collective operations[17]. Benchmark tests indicate that the code currently scales up to at least 256 CPUS on JUMP and 1024 CPUs on the new BlueGene/L architecture – Fig.4.

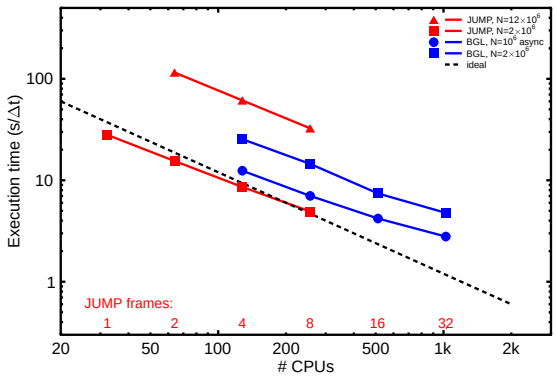

Figure 4. Timings on IBM-p690 cluster and BlueGene/L for multi-million charge spheres.

6 Concluding Remarks

Although slower than their mesh-based particle-in-cell equivalents, parallel tree codes offer exciting new possibilities in plasma simulation, particularly where collisions are important; for modelling complex geometries; or for mass-limited systems in which artificial boundaries would severely compromise the simulation's validity. The generic nature of this algorithm, combined with excellent parallel scalability, means that it can be easily adapted to other systems dominated by long-range interactions.

Acknowledgments

The author gratefully acknowledges support in performance issues from Bernd Mohr, Wolfgang Frings (ZAM) and Christoph Pospiech (of ACTC, IBM); and Sonja Dominiczak (ZAM) for assistance with visualisation. Simulations were performed with computing resources granted by the VSR of the Research Centre Jülich under project JZAM04.

References

1. J. Barnes and P. Hut, *A hierarchical $O(N \log N)$ force-calculation algorithm*, Nature **324**, 446–449 (1986).
2. S. Pfalzner and P. Gibbon, *Direct calculation of inverse-bremsstrahlung absorption in strongly coupled, nonlinearly driven laser plasmas.*, Phys. Rev. E **57**, 4698–4705 (1998).
3. P. Gibbon, *Short Pulse Laser Interactions with Matter: An Introduction*, Imperial College Press/World Scientific London/Singapore (September 2005), ISBN 1-86094-135-4 (hardback).
4. S. Pfalzner and P. Gibbon, *Many Body Tree Methods in Physics*, Cambridge University Press New York (1996).

5. H. Okuda and C. K. Birdsall, *Collisions in a plasma of finite-size particles*, Phys. Fluids **13**, 2123–2134 (1970).
6. P. Gibbon, *Resistively enhanced proton acceleration via high-intensity laser interactions with cold foil targets*, Phys. Rev. E **72**(026411), 1–8 (2005).
7. P. Gibbon, F. N. Beg, R. G. Evans, E. L. Clark, , and M. Zepf, *Tree code simulations of proton acceleration from laser-irradiated wire targets*, Phys. Plasmas **11**, 4032–4040 (2004).
8. A. Pukhov, *Three-dimensional simulations of ion acceleration from a foil irradiated by a short-pulse laser*, Phys. Rev. Lett. **86**, 3562–3565 (2001).
9. A. R. Bell, J. R. Davies, S. Guérin, and H. Ruhl, *Fast-electron transport in high-intensity short-pulse laser-solid experiments*, Plasma Phys. Control. Fusion **39**, 653–659 (1997).
10. D. Batani, A. Antonicci, F. Pisani, T. A. Hall, D. Scott, F. Amiranoff, M. Koenig, L. Gremillet, S. Baton, E. Martinolli, C. Rousseaux, and W. Nazarov, *Inihibition in the propagation of fast electrons in plasma foams by resistive electric fields*, Phys. Rev. E **65** (2002).
11. J. R. Davies, A. R. Bell, M. G. Haines, and S. M. Guérin, *Short-pulse hight-intensity laser-generated fast electron transport into thick solid targets*, Phys. Rev. E **56**, 7193–7203 (1997).
12. T. Z. Esirkepov, S. V. Bulanov, K. Nishihara, T. Tajima, F. Pegoraro, V. S. Khoroshkov, K. Mima, H. Daido, Y. Kato, Y. Kitagawa, K. Nagai, and S. Sakabe, *Proposed double-layer target for the generation of high-quality laser-accelerated ion beams*, Phys. Rev. Lett. **89**, 175003 (2002).
13. F. N. Beg, M.-S. Wei, A. E. Dangor, A. Gopal, M. Tatarakis, K. Krushelnick, P. Gibbon, E. L. Clark, R. G. Evans, K. L. Lancaster, P. A. Norreys, K. W. D. Ledingham, P. McKenna, and M. Zepf, *Target charging effects on proton acceleration during high intensity short pulse laser-solid interactions*, Appl. Phys. Lett. **84**, 2766–2768 (2003).
14. F. N. Beg, E. L. Clark, M.-S. Wei, A. E. Dangor, R. G. Evans, P. Gibbon, A. Gopal, K. L. Lancaster, P. A. Norreys, M. Tatarakis, M. Zepf, and K. Krushelnick, *Return current and proton emission from short pulse laser interactions with wire targets*, Phys. Plasmas **11**, 2806–2813 (2004).
15. S. Pfalzner and P. Gibbon, *A hierarchical tree code for dense plasma simulation*, Comp. Phys. Commun. **79**, 24–38 (1994).
16. M. S. Warren and J. K. Salmon, *A portable parallel particle program*, Comp. Phys. Commun. **87**(266–290) (1995).
17. P. Gibbon, W. Frings, S. Dominiczak, and B. Mohr, *Performance analysis and visualization of the N-body tree code PEPC on massively parallel computers*, Proc. Parallel Computing 2005, Malaga (2005).